Modeling Neural Mechanisms for Genesis of Respiratory Rhythm and Pattern. I. Models of Respiratory Neurons

ILYA A. RYBAK, JULIAN F. R. PATON, AND JAMES S. SCHWABER
Central Research Department, DuPont Experimental Station E-328/B31, Delaware 19880-0328; and Department of Physiology, School of Medical Sciences, University of Bristol, Bristol BS8 1TD, United Kingdom

Rybak, Ilya A., Julian F. R. Paton, and James S. Schwaber. Modeling neural mechanisms for genesis of respiratory rhythm and pattern. I. Models of respiratory neurons. *J. Neurophysiol.* 77: 1994–2006, 1997. The general objectives of our research, presented in this series of papers, were to develop a computational model of the brain stem respiratory neural network and to explore possible neural mechanisms that provide the genesis of respiratory oscillations and the specific firing patterns of respiratory neurons. The present paper describes models of single respiratory neurons that have been used as the elements in our network models of the central respiratory pattern generator presented in subsequent papers. The models of respiratory neurons were developed in the Hodgkin-Huxley style employing both physiological and biophysical data obtained from brain stem neurons in mammals. Two single respiratory neuron models were developed to match the two distinct firing behaviors of respiratory neurons described in vivo: neuron type I shows an adapting firing pattern in response to synaptic excitation, and neuron type II shows a ramp firing pattern during membrane depolarization after a period of synaptic inhibition. We found that a frequency ramp firing pattern can result from intrinsic membrane properties, specifically from the combined influence of calcium-dependent $K_{AHP}(Ca)$, low-threshold Ca_T and K_A channels. The neuron models with these ionic channels (type II) demonstrated ramp firing patterns similar to those recorded from respiratory neurons in vivo. Our simulations show that $K_{AHP}(Ca)$ channels in combination with high-threshold Ca_L channels produce spike frequency adaptation during synaptic excitation. However, in combination with low-threshold Ca_T channels, they cause a frequency ramp firing response after release from inhibition. This promotes a testable hypothesis that the main difference between the respiratory neurons that adapt (for example, early inspiratory, postinspiratory, and decrementing expiratory) and those that show ramp firing patterns (for example, ramp inspiratory and augmenting expiratory) consists of a ratio between the two types of calcium channels: Ca_L channels predominate in the former and Ca_T channels in the latter respiratory neuron types. We have analyzed the dependence of adapting and ramp firing patterns on maximal conductances of different ionic channels and values of synaptic drive. The effect of adjusting specific membrane conductances and synaptic interactions revealed plausible neuronal mechanisms that may underlie modulatory effects on respiratory neuron firing patterns and network performances. The results of computer simulation provide useful insight into functional significance of specific intrinsic membrane properties and their interactions with phasic synaptic inputs for a better understanding of respiratory neuron firing behavior.

INTRODUCTION

Genesis of the respiratory rhythm: paradigms and models

This paper is the first in a series describing our efforts to understand mechanisms for respiratory rhythm and pattern generation at the cellular, network, and system levels using modeling methods. The respiratory rhythm generator is located in a relatively small area of the lower brain stem (Lumsden 1923; for review see also: Feldman 1986; Richter 1986a; von Euler 1986). Although undetermined, the genesis of the primary respiratory oscillations likely is to be defined by intrinsic and/or network properties of neurons within this limited area. Feldman and Cleland (1982) and Smith et al. (1991) have suggested pacemaker-like activity as being responsible for generating the primary respiratory oscillations (a ''pacemaker paradigm''). Alternatively a ''network paradigm'' suggests that the respiratory rhythm results from reciprocal inhibitory interactions between different respiratory neuron types (Balis et al. 1994; Botros and Bruce 1990; Geman and Miller 1976; Gottschalk et al. 1994; Ogilvie et al. 1992; Richter and Ballantyne 1983; Richter et al. 1986a; Rubio 1972). The network basis does not exclude intrinsic membrane properties of neurons playing an important role in respiratory rhythmogenesis. Recent data allow the conclusion that membrane ionic channels may control both the timing of onset and patterns of neuronal discharges (Champagnat and Richter 1994; Mifflin et al. 1985; Pierrefiche et al. 1995; Richter et al. 1985, 1986b, 1993). However, a definitive role of intrinsic membrane properties of neurons in generation of both respiratory rhythm and pattern remains unresolved.

To date, network models of respiratory rhythmogenesis have been based on relatively simple models of single neurons (Botros and Bruce 1990; Duffin 1991; Duffin et al. 1995; Feldman and Cowan 1975; Geman and Miller 1976; Gottschalk et al. 1994; Ogilvie et al. 1992; Rubio 1972). These models considered network mechanisms for respiratory rhythmogenesis and did not explore the role of intrinsic neuronal properties. It is not possible, therefore, to use these models for comparing simulated versus experimentally recorded membrane trajectories and firing patterns of single respiratory neurons. Recent intracellular data (Bryant et al. 1993; Champagnat and Richter 1994; Champagnat et al. 1986b,c; Dekin and Getting 1987; Haddad and Getting 1989; Mifflin et al. 1985; Paton 1996; Pierrefiche et al. 1995; Richter et al. 1985, 1986b, 1993; Schwarzacher et al. 1991) together with modern computational approaches for simulating ''biological'' neurons (Huguenard and McCormick 1991, 1992; McCormick and Huguenard 1992; Schwaber et al. 1993; Yamada et al. 1989) provide an opportunity to develop more realistic and predictive models of respiratory neurons and a respiratory network.

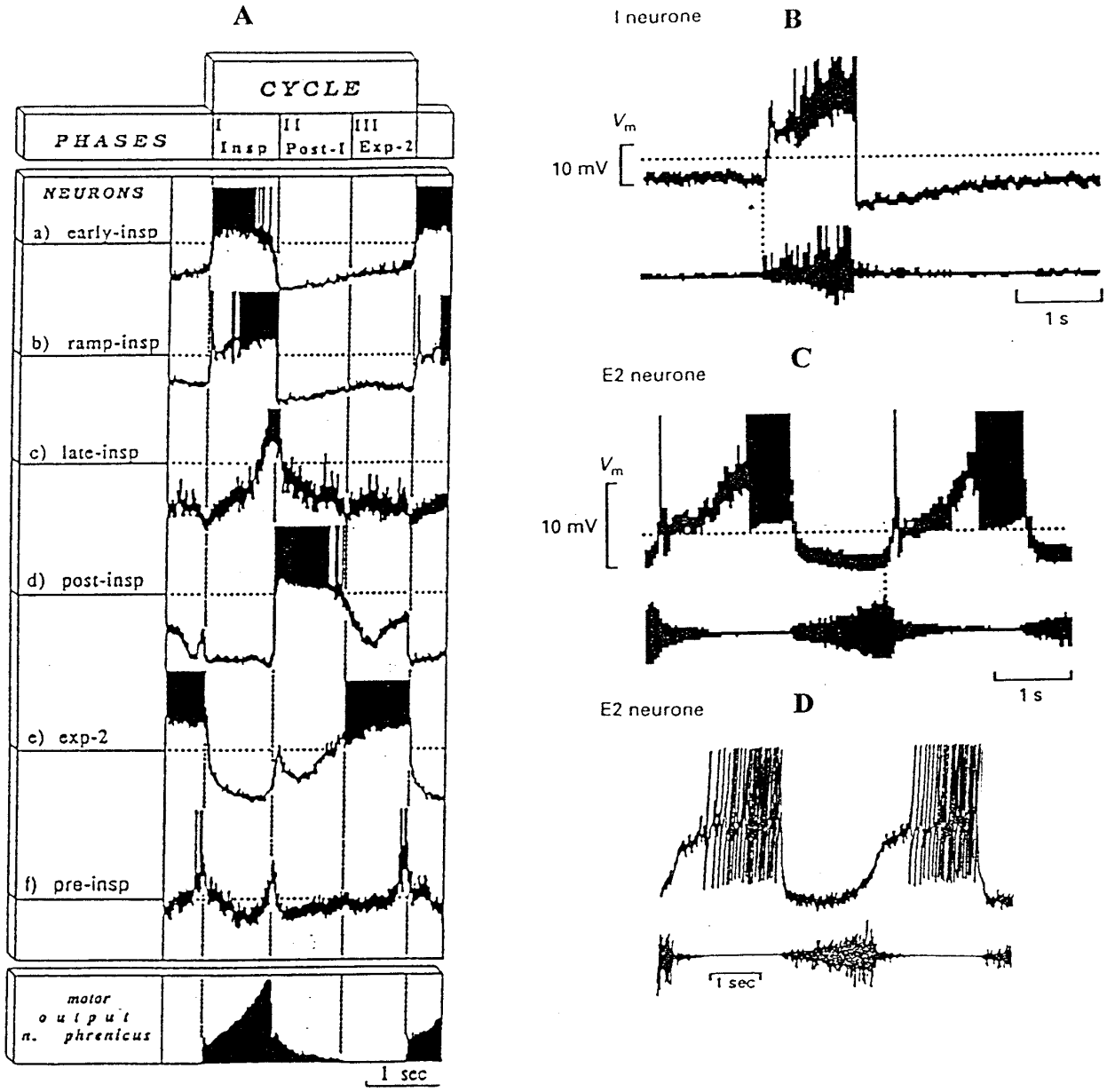

FIG. 1. Activity patterns of different types of respiratory neurons recorded intracellulary in vivo. *A*: normalized recordings of membrane potential trajectories and firing response patterns of different respiratory neurons (taken from Richter 1996). *B*: firing pattern of an inspiratory neuron: rebound depolarization occurs after neuron is released from inhibition (Richter et al. 1993). *C* and *D*: firing patterns of 2 expiratory neurons (*C* from Richter et al. 1993; *D* from Klages et al. 1993).

The main objectives of this study were to develop single neuron models based on available experimental data and investigate the significance of certain membrane ionic channels for producing the characteristic firing patterns associated with different respiratory neuron types.

Activity patterns of respiratory neurons

The respiratory cycle has been considered to comprise three phases: inspiratory, postinspiratory (stage I expiration), and expiratory (stage II expiration) (Richter 1996; Richter and Ballantyne 1983; Richter et al. 1986a) which are seen in the phrenic neurogram (Fig. 1*A*). Respiratory neurons usually are classified into types, depending on their firing pattern and phase relative to the phrenic cycle. Respiratory neurons described in vivo include, for example, early inspiratory (early-I); ramp inspiratory (ramp-I); late inspiratory (late-I); postinspiratory (post-I); stage II expiratory (E2); preinspiratory (pre-I) (Fig. 1) (Botros and Bruce 1990; Feldman 1986; Gottschalk et al. 1994; Ogilvie et al. 1992; Richter 1996; Richter and Ballantyne 1983; Richter et al. 1986a); decrementing (dec-E) and augmenting (aug-E) expiratory neurons (Balis et al. 1994; Bryant et al. 1993; Ezure 1990).

The typical discharge patterns recorded from respiratory neurons include an adapting (or decrementing) firing pattern, showing a decrease in spike frequency during the burst, and a ramp (or augmenting) firing pattern in which the frequency

increases with time. The adapting bursts are typical for early-I and post-I neurons (Fig. 1*A*) (Richter 1996; Richter and Ballantyne 1983; Richter et al. 1986a) and dec-E neurons (Bryant et al. 1993). The ramp firing patterns are observed in inspiratory neurons including ramp-I neurons (Fig. 1, *A* and *B*) and some expiratory neurons like E2 (Fig. 1, *A, C,* and *D*) (Richter and Ballantyne 1983; Richter et al. 1986a) or aug-E neurons (Bryant et al. 1993; Ezure 1990; Feldman 1986; von Euler 1986). The duration of the patterns is noteworthy, because each may extend for at least a respiratory phase, i.e., from several hundred milliseconds to seconds.

The ramp firing patterns usually occur when neurons are released from inhibition and often follow a postinhibitory rebound excitation. Inspiratory neurons display such sudden rebound membrane excitation when released from synaptic inhibition during the transition from expiration to inspiration (Richter et al. 1993) (Fig. 1*A* for ramp-I; Fig. 1*B*). Expiratory neurons reveal a similar trajectory in their membrane potentials on release from synaptic inhibition (Richter et al. 1993) (Fig. 1*C*). This rebound depolarization can trigger one or two action potentials (Fig. 1*A* for ramp-I, Fig. 1, *B* and *C*). Interestingly, a period of silence characteristically follows the rebound spike(s) (Fig. 1*A* for ramp-I, Fig. 1*B*).

Adapting and ramp firing patterns might result either from synaptic interactions and/or intrinsic cellular properties. For example, changes in spiking frequency of some neurons may reflect simple alterations in excitatory or inhibitory synaptic drive. Most models of the respiratory network assume that adapting patterns result from intrinsic properties of the neurons (Botros and Bruce 1990; Duffin 1991; Duffin et al. 1995; Geman and Miller 1976; Gottschalk et al. 1994; Ogilvie et al. 1992; Rubio 1972). This suggestion is plausible because adapting response patterns are not a specific feature of respiratory neurons but are found in neurons throughout the nervous system. In contrast, ramp firing activity is a highly unusual property of central neurons. Most theories and models of respiratory rhythmogenesis try to explain this property on the basis of network interactions alone. For example, it is proposed that the frequency increase in ramp-I neurons is based on collateral self-excitation or mutual synaptic excitation between neurons of the same group (Botros and Bruce 1990; Feldman and Cowan 1975; Gottschalk et al. 1994; Ogilvie et al. 1992). Alternatively, the ramp (augmenting) firing pattern of expiratory neurons are often explained as a result of disinhibition from adapting respiratory neurons. However, no model has been able to reproduce successfully the physiological ramp firing patterns of inspiratory and expiratory neurons (recorded in vivo; see Fig. 1, *A*–*C*) using network properties alone and in no model were intrinsic neuronal properties considered as a mechanism underlying the ramp firing patterns. These were the primary reasons for our decision to develop more realistic single respiratory neuron models in the Hodgkin-Huxley tradition by incorporating all available biophysical data.

Membrane properties of respiratory neurons

Modern intracellular approaches have provided direct (in vivo) and indirect (in vitro) evidence for the existence of different voltage- and time-dependent ionic channels in respiratory neurons (Bryant et al. 1993; Champagnat and Richter 1994; Champagnat et al. 1986b,c; Dekin and Getting 1987; Haddad and Getting 1989; Mifflin et al. 1985; Pierrefiche et al. 1995; Richter et al. 1985, 1986b, 1993). Specifically, transient potassium (A-type, K_A), calcium-dependent potassium [K(Ca)], high-threshold (Ca_L) and transient low-threshold (Ca_T) calcium channels have been reported. These membrane channels may determine the different firing patterns of respiratory neurons and control respiratory network performance. Mifflin et al. (1985) concluded that the K(Ca) conductance produced a time-dependent decrease in firing frequency that may account for the adaptation seen in early-I and post-I neurons after an initial high-frequency discharge (Richter et al. 1993). The rebound membrane depolarization, that inspiratory and expiratory neurons usually display on releasing from synaptic inhibition (Fig. 1, *B* and *C*), results most likely from Ca_T channels (Richter et al. 1993).

METHODS

Single neuron models

Our single neuron models are typical single compartment models. They have been developed using the Hodgkin-Huxley formalism (Hodgkin and Huxley 1952). The neuron membrane potential V is described as follows

$$c \cdot \frac{d}{dt} V = \sum_i g_i \cdot (E_i - V) + I \qquad (1)$$

where c is the neuron membrane capacitance; t is time; I is the injected current (in the case of synaptic inputs $I=0$); g_i and E_i are the conductance and reversal potential of the channel i, respectively.

The set of membrane channels includes: specific Na^+, K^+, and Ca^{2+} ionic channels; the leakage channel (L); excitatory (SynE) and inhibitory (SynI) synaptic channels.

Following the Hodgkin-Huxley formalism, conductances of ionic channels are represented in the following form

$$g_i = \bar{g}_i \cdot m_i^{\alpha_i}(V, t) \cdot h_i^{\beta_i}(V, t)$$

$$\tau_{m_i}(V) \cdot \frac{d}{dt} m_i = m_{\infty i}(V) - m_i$$

$$\tau_{h_i}(V) \cdot \frac{d}{dt} h_i = h_{\infty i}(V) - h_i \qquad (2)$$

where $\bar{g}_i$ is the maximal conductance of the channel i; m_i and h_i are the variables that define dynamics of, respectively, activation and inactivation of the channel i; α_i and ß$_i$ are the powers of m_i and h_i, respectively. The steady state values of m_i and h_i ($m_{\infty i}$ and $h_{\infty i}$), and their time constants (τ_{m_i} and τ_{h_i}) depend generally on the membrane potential V, and in some cases on calcium concentration inside the cell, $[Ca^{2+}]_{in}$.

The following ionic channels have been included in the model: fast sodium channels, Na_{fast} ($g_i = g_{Na}$); delayed rectifier potassium channels, K_{DR} ($g_i = g_{DR}$); transient potassium-A channels, K_A ($g_i = g_A$); calcium-dependent potassium channels, which provide long-lasting afterhyperpolarization, K_{AHP}(Ca) ($g_i = g_{AHP}$); high-threshold Ca_L ($g_i = g_{CaL}$) and low-threshold Ca_T ($g_i = g_{CaT}$) calcium channels. The Na_{fast} and K_{DR} channels are necessary for generation of action potentials and are presented in all spiking neurons. The K_A, K_{AHP}(Ca), Ca_L, and Ca_T channels have been incorporated into the model because of evidence of their presence and specific function in various types of respiratory neurons (see INTRODUCTION). The leakage conductance is considered as a constant, $g_i = g_L = \bar{g}_L$.

In general, excitatory and inhibitory input signals to a neuron model can be applied in two ways: either via positive or negative changes of the injected current I, which is equal to 0 at rest (i.e., in the absence of input signals), or by changing synaptic excitatory ($g_i = g_{SynE}$) and inhibitory ($g_i = g_{SynI}$) conductances, which are also equal to 0 at rest. We chose the latter method because it is more physiological and allows consideration of the neuron as an element in a network of synaptically connected neurons.

The reversal potentials for sodium, potassium, and calcium channels are defined by the Nernst equation

$$E_i = \frac{R \cdot T}{z_i \cdot F} \cdot \ln \frac{[X_i]_{out}}{[X_i]_{in}} \quad (3)$$

where R is the gas constant; T is the temperature in degrees Kelvin; z_i is the valence of the ion i; F is Faraday's constant; $[X_i]_{out}$ is the concentration of the ions i outside the cell; $[X_i]_{in}$ is the concentration of the ions i below the membrane inside the cell. The reversal potentials for sodium (E_{Na}) and potassium (E_K) channels usually are considered constant in models of the Hodgkin-Huxley style (Hodgkin and Huxley 1952; Huguenard and McCormick 1991, 1992; McCormick and Huguenard 1992; Schwaber et al. 1993) and may be calculated from *Eq. 3*. Due to the strong dependence of the calcium reversal potential (E_{Ca}) and calcium-dependent potassium currents on $[Ca^{2+}]_{in}$, the latter is considered one of the main model variables. Therefore, in our model, E_{Ca} is not constant but depends on $[Ca^{2+}]_{in}$ in accordance with *Eq. 3*. The reversal potentials for the synaptic (E_{SynE} and E_{SynI}) and the leakage (E_L) channels are constant. The value of E_L has been tuned to provide the required resting membrane potential in the absence of input signals.

Incorporating calcium and calcium-dependent channels into the model requires a description of the dynamics of free calcium concentration below the membrane (inside a so-called ''thin shell''; $d = 0.1$ μm) (Yamada et al. 1989). Free calcium ions enter the shell by influx through voltage-gated calcium channels after which they are buffered and pumped out of the neuron. Dynamics of free calcium concentration inside the shell are described by the following differential equation (Schwaber et al. 1993)

$$\frac{d}{dt}[Ca^{2+}]_{in} = \frac{I_{Ca}}{2 \cdot F \cdot v} \cdot (1 - P_B) + \frac{[Ca^{2+}]_{in0} - [Ca^{2+}]_{in}}{\tau_{pump}(V)} \quad (4)$$

where the first term constitutes influx and buffering, and the second term describes pump kinetics; v is the volume of the shell, with a thickness of $d = 0.1$ μm and an area equal to the area of neuronal membrane, Ω: $v = d \cdot \Omega$.

Influx is provided by the calcium current I_{Ca} through all calcium channels

$$I_{Ca} = (g_{CaL} + g_{CaT}) \cdot (E_{Ca} - V) \quad (5)$$

Buffering is modeled as an instantaneous process (Eckert and Chad 1984; Schwaber et al. 1993). The influx is multiplied by the $(1 - P_B)$, where P_B is the probability of a Ca^{2+} ion being buffered when it enters the shell. Buffering can be considered as the second-order reaction with the forward rate f and backward rate b (Yamada et al. 1989)

$$B + Ca^{2+} \underset{b}{\overset{f}{\Leftrightarrow}} CaB \quad (6)$$

The reaction can be described as follows

$$\frac{d}{dt}[Ca^{2+}] = \frac{d}{dt}[B] = b \cdot [Ca \cdot B] - f \cdot [Ca^{2+}] \cdot [B] \quad (7)$$

The sum of concentrations of free $[B]$ and bound $[B \cdot Ca]$ buffer are considered to be constant

$$[B] + [B \cdot Ca] = [B]_{Total} \quad (8)$$

For the stationary state of *Eq. 7*, the expression for bound calcium $[Ca \cdot B]$ can be derived from *Eqs. 7* and *8*

$$[Ca \cdot B] = \frac{[Ca^{2+}] \cdot [B]_{Total}}{[Ca^{2+}] + K} \quad (9)$$

where $K = b/f$.

The probability of Ca^{2+} ion buffering can be derived as follows

$$P_B = \frac{[Ca \cdot B]}{[Ca^{2+}] + [Ca \cdot B]} = \frac{[B]_{Total}}{[Ca^{2+}] + [B]_{Total} + K} \quad (10)$$

In the second term of *Eq. 4* describing pumping, $[Ca^{2+}]_{in0}$ is the equilibrium Ca^{2+} concentration of the pump, $\tau_{pump}(V)$ is the pump's time constant, which depends on the membrane potential (Yamada et al. 1989)

$$\tau_{pump} = 17.7 \cdot \exp(V/35) \quad (11)$$

Choices of model parameters and ionic channel kinetics

Ideally the parameters and kinetics for our Hodgkin-Huxley type models would be drawn from experimental data obtained from characterized brain stem respiratory neurons. However, these data are incomplete for respiratory neurons. Therefore, we first used all available data on characterized respiratory neurons and noncharacterized neurons from respiratory related brain stem areas and then adapted experimental data from other closely related neuron classes. In doing so, we have accounted for species differences, membrane properties such as resting membrane potential, and temperature to which the experimental data or channel kinetics descriptions were related. This ensured that the resulting membrane voltage dynamics in our models were not the result of unrealistic parameter interactions but reflected the specific characteristics of modeled neurons or kinetic properties of ionic channels. The formal descriptions of channel kinetics were drawn from the models of rat thalamic relay and cortical pyramidal neurons by Huguenard and McCormick (Huguenard and McCormick 1991, 1992; McCormick and Huguenard 1992). The expressions used for conductances of ionic channels, g_i, their steady state values, $m_{\infty i}$ and $h_{\infty i}$, and time constants, τ_{m_i} and τ_{h_i}, are presented in Table 1. Specific values of membrane area, resistance, and capacitance were taken or drawn from measurements in cardiorespiratory region of the brain stem. All parameters were corrected to the Huguenard and McCormick (1992) temperature of $T = 308$ K (35°C). Units for the model variables and parameters are presented in Table 2.

The area of the somatic membrane of a medium respiratory neuron used in the model was $\Omega = 0.0025$ mm^2. It was based on the experimental data of Champagnat et al. (1986b) in which the average diameter of somata was 20–30 μm, and the data of Kreuter et al. (1977) in which the average somata area was 3,800 μm^2 for bulbospinal neurons and 1,800 μm^2 for other respiratory neurons. The membrane capacitance, $c = 0.025$ nF, was calculated on the basis of the area of the membrane and an accepted value for specific capacitance of 1 μF/cm^2 (Hille 1984). The same value of capacitance may be obtained by dividing the membrane time constant, $\tau_m = 2.5$ ms, which is close to the measured values in Kreuter et al. (1977) by the input resistance of the membrane, $R_i = 100$ MΩ [50–150 MΩ in Champagnat et al. (1986b) and 60–150 MΩ in Haddad and Getting (1989)].

Reversal potential for the Na_{fast} channel was set to $E_{Na} = 55$ mV (Huguenard and McCormick 1992). According to *Eq. 3* and taking into account the temperature and values of the constants: $R = 8.3143 \cdot 10^3$ J/(Kmol·K) and $F = 9.648 \cdot 10^4$ C/mol, this value corresponds to the ratio $[Na^+]_{out}/[Na^+]_{in} = 8$. The reversal potential for the potassium channels [K_{DR}, K_A, and $K_{AHP}(Ca)$], $E_K = -94$ mV, was calculated from *Eq. 3* at $T = 308$ K, $[K^+]_{out} = 4$ mM, and $[K^+]_{in} = 140$ mM (Yamada et al. 1989). The accepted value for external concentration of calcium ions was $[Ca^{2+}]_{out} =$

TABLE 1. *Expressions for conductances of ionic channels used in respiratory neuron models*

Channel	Conductance, g_i	Description of Parameters
Fast sodium, Na_{fast}	$g_{Na} = \bar{g}_{Na} \cdot m_{Na}^3 \cdot h_{Na}$	$m_{\infty Na} = \dfrac{0.091 \cdot (V + 38)/(1 - \exp(-(V + 38)/5)}{0.091 \cdot (V + 38)/(1 - \exp(-(V + 38)/5)) + 0.062 \cdot (V + 38)/(\exp((V + 38)/5) - 1)}$
		$\tau_{mNa} = 1/(0.091 \cdot (V + 38)/(1 - \exp(-(V + 38)/5)) + 0.062 \cdot (V + 38)/(\exp((V + 38)/5) - 1))$
		$h_{\infty Na} = \dfrac{0.016 \cdot \exp(-(V + 55)/15)}{0.016 \cdot \exp(-(V + 55)/15) + 2.07/(1 + \exp(-(V - 17)/21)}$
		$\tau_{hNa} = 1/(0.016 \cdot \exp(-(V + 55)/15) + 2.07/(1 + \exp(-(V - 17)/21))$
Potassium-delayed rectifier, K_{DR}	$g_{DR} = \bar{g}_{DR} \cdot m_{DR}^4$	$m_{\infty DR} = \dfrac{0.01 \cdot (V + 45)/(1 - \exp(-(V + 45)/5))}{0.01 \cdot (V + 45)/(1 - \exp(-(V + 45)/5)) + 0.17 \cdot \exp(-(V + 50)/40)}$
		$\tau_{mDR} = 1/(0.01 \cdot (V + 45)/(1 - \exp(-(V + 45)/5)) + 0.17 \cdot \exp(-(V + 50)/40))$
Transient potassium-A, K_A	$g_A = \bar{g}_A \cdot (0.6 \cdot m_{A1}^4 \cdot h_{A1} + 0.4 \cdot m_{A2}^4 \cdot h_{A2})$	$m_{\infty A1} = 1/(1 + \exp(-(V + 60)/8.5))$ $\tau_{mA1} = 1/(\exp((V + 35.82)/19.69) + \exp(-(V + 79.69)/12.7) + 0.37)$ $h_{\infty A1} = 1/(1 + \exp((V + 78)/6))$ $\tau_{hA1} = 1/(1 + \exp((V + 46.05)/5) + \exp(-(V + 238.4)/37.45))$ if $V < -63$, else $\tau_{hA1} = 19.0$ $m_{\infty A2} = 1/(1 + \exp(-(V + 36)/20))$ $\tau_{mA2} = 1/(\exp((V + 35.82)/19.69) + \exp(-(V + 79.69)/12.7) + 0.37)$ $h_{\infty A2} = 1/(1 + \exp((V + 78)/6))$ $\tau_{hA2} = 1/(1 + \exp((V + 46.05)/5) + \exp(-(V + 238.4)/37.45))$ if $V < -73$, else $\tau_{hA2} = 60.0$
Calcium-dependent potassium, K_{AHP}	$g_{AHP} = \bar{g}_{AHP} \cdot m_{AHP}^2$	$m_{\infty AHP} = 1.25 \cdot 10^8 \cdot [Ca^{2+}]_{in}^2/(1.25 \cdot 10^8 \cdot [Ca^{2+}]_{in}^2 + 2.5)$ $\tau_{mAHP} = 1{,}000/(1.25 \cdot 10^8 \cdot [Ca^{2+}]_{in}^2 + 2.5)$
High-threshold calcium, Ca_L	$g_{CaL} = \bar{g}_{CaL} \cdot m_{CaL}^2$	$m_{\infty CaL} = \dfrac{1.6/(1 + \exp(-0.072 \cdot (V - 5)))}{1.6/(1 + \exp(-0.072 \cdot (V - 5))) + 0.02 \cdot (V - 1.31)/(\exp((V - 1.31)/5.36) - 1)}$
		$\tau_{mCaL} = 1/(1.6/(1 + \exp(-0.072 \cdot (V - 5))) + 0.02 \cdot (V - 1.31)/(\exp((V - 1.31)/5.36) - 1))$
Low-threshold calcium, Ca_T	$g_{CaT} = \bar{g}_{CaT} \cdot m_{CaT}^2 \cdot h_{CaT}$	$m_{\infty CaT} = 1/(1 + \exp(-(V + 60.5)/6.2))$ $\tau_{mCaT} = 0.612 + 1/(1 + \exp(-(V + 131.6)/16.7) + \exp((V + 16.8)/18.2))$ $h_{\infty CaT} = 1/(1 + \exp((V + 84.5)/4.03))$ $\tau_{hCaT} = \exp((V + 467)/66.6)$ if $V < -80$, else $\tau_{hCaT} = 28 + \exp(-(V + 21.88)/10.52)$

The expressions for conductances of all ionic channels have been taken from the models of Huguenard and McCormick (1991, 1992) except those for the calcium-dependent potassium conductance. The latter are taken from Yamada et al. (1989).

4 mM (Yamada et al. 1989). Thus, the calcium reversal potential obtained from *Eq. 3* is a function of $[Ca^{2+}]_{in}$

$$E_{Ca} = 13.27 \cdot \ln (4/[Ca^{2+}]_{in}) \quad (12)$$

The equilibrium concentration of calcium ions inside the shell below the membrane was set at $[Ca^{2+}]_{in0} = 5 \cdot 10^{-5}$ mM (Yamada et al. 1989). So, at rest $E_{Ca} = 150$ mV. The reversal potentials for the excitatory synaptic channels was $E_{SynE} = -10$ mV (Yamada et al. 1989). The reversal potential for the inhibitory synaptic channels was set equal to that for the potassium channels ($E_{SynI} = E_K = -94$ mV) because some in vivo recordings demonstrated inhibitory hyperpolarization below the chloride reversal potential (Richter et al. 1993). The additional justification for this was that activation of γ-aminobutyric acid-B receptors (associated with potassium inhibitory synapses) decreased the activity of all types of respiratory neurons (Pierrefiche et al. 1993). The leakage conductance was $g_L = 0.01$ μS to be consistent with the used input resistance of the membrane R_i (see above). We tuned the value of E_L to obtain a resting membrane potential $V_{rest} = -60$ mV (Haddad and Getting 1986; Richter et al. 1993).

TABLE 2. *Units*

Type of Variable	Unit
Voltage	mV
Current	nA
Conductance	μS (MΩ^{-1})
Capacitance	nF
Concentration	mM
Volume	nl
Time	ms

The following parameters were set to define the dynamics of free calcium concentration inside the shell below the membrane: $v = d \cdot \Omega = 2.5 \cdot 10^{-4}$ nl; $[Ca^{2+}]_{in0} = 5 \cdot 10^{-5}$ mM; $B_{total} = 0.030$ mM; $K = 0.001$ mM (Yamada et al. 1989).

The dynamics of synaptic stimulation are described as follows

$$\tau_E \cdot \frac{d}{dt} g_{SynE} = -g_{SynE} + In_E$$

$$\tau_I \cdot \frac{d}{dt} g_{SynI} = -g_{SynI} + In_I \quad (13)$$

where variables In_E and In_I (In_E, $In_I \geq 0$) define the amplitudes of excitatory and inhibitory synaptic stimulation respectively; τ_E and τ_I are, correspondingly, the time constants of stimulation. The dynamic type of stimulation allowed investigation of the functional significance of both the dynamics of synaptic processes and external stimulation.

Our simulations were performed using the MacGregor's integration method for the solution of membrane differential equations (MacGregor 1987). To be sure that the obtained results are independent of the used integration method, we checked many of our results using the fourth-order Runge-Kutta integration method. Through these simulation experiments, we concluded that for our models the MacGregor's method has good stability and accuracy characteristics at the integration step of $\leq$0.1 ms, and we have followed this practice throughout for the results of the present paper.

RESULTS

Using the above descriptions and values of parameters, we have structured two specific types of single neuron mod-

els that accurately reproduce the adapting and ramp firing patterns of respiratory neurons. We began with a model that lacks calcium channels to explore and determine the role of voltage-sensitive potassium channels in our respiratory neuron models. Then we incorporated calcium and calcium-dependent potassium channels to explore the possible role of these channels in the firing behavior of different respiratory neurons.

A basic neuron model: the role of K_A channels

The basic neuron model contains the following ionic channels: fast sodium, Na_{fast}; delayed rectifier potassium, K_{DR}; transient potassium A, K_A; and leakage, L. The following maximal conductances have been set for these channels: $\bar{g}_{Na} = 3.0\ \mu S$; $\bar{g}_{DR} = 0.90\ \mu S$; $\bar{g}_A = 0.15\ \mu S$; $\bar{g}_L = 0.01\ \mu S$. The maximal conductances for the sodium ($\bar{g}_{Na} = 3.00\ \mu S$) and delayed rectifier potassium ($\bar{g}_{DR} = 0.90\ \mu S$) channels have been calculated using the values of specific conductances from the classical model of Hodgkin and Huxley (1952) (120 mS/sm^2 and 36 mS/sm^2, respectively), and the accepted area of neuronal membrane ($\Omega = 0.0025$ mm^2).

The maximal conductance of K_A channels found in neurons of the nuclei of the solitary tract of rat brain stem slices was in the range of 0.02–0.07 μS (Champagnat et al. 1986b,c). This was determined from the amplitude of the K_A current measured when neurons were released from a hyperpolarized state. However, we set $\bar{g}_A = 0.15\ \mu S$, which is twice that reported. This was necessary to achieve the same maximal K_A current in simulation under similar conditions. The K_A channels, used in our model, consisted of two different subpopulations (see Table 1). This is consistent with in vitro observations (Dekin and Getting 1987). However, the second subpopulation of K_A channels (which comprised 40% of the total K_A) did not influence the neuron behavior in our simulations. This was the additional justification for doubling the $\bar{g}_A$ value.

The basic neuron model shows a regular spike train at a constant frequency in response to constant excitatory synaptic drive exceeding the firing threshold. The relationship between the spiking frequency of the basic neuron model and the amount of excitatory synaptic input is shown in Fig. 2 (solid line). Our simulation confirmed the generally accepted functional roles of K_A channels: providing a low frequency firing and a linear relationship between input and spike frequency (Connor and Stevens 1971). Figure 2 shows that without K_A channels, a threshold stimulus initiates a 40-Hz firing rate, and the frequency-input curve becomes nonlinear. Increasing of $\bar{g}_A$ allows the neuron model to generate low-frequency spike trains (from 2 to 5 Hz) and produces a linear frequency-input curve.

An adapting neuron (type I): The role of Ca_L, $K(Ca)_{AHP}$, and K_A channels

It is known that a combination of $K_{AHP}(Ca)$ and Ca_L channels can provide an adaptive frequency response during depolarization (Huguenard and McCormick 1992; Yamada et al. 1989). To simulate spike frequency adaptation, we have developed a *neuron type I* model by incorporating these channels into the basic neuron. The maximal conductances of neuron type I are presented in Table 3. We set the maximal conductances of $K_{AHP}(Ca)$ and Ca_L channels equal to $\bar{g}_{AHP} = 0.15\ \mu S$ and $\bar{g}_{CaL} = 0.0015\ \mu S$, respectively. These values optimally reproduced the rate of spike frequency adaptation reported for respiratory neurons.

An example of adapting response of neuron type I to step excitatory input is shown in Fig. 3. The mechanism for spike frequency adaptation in our model is the following: synaptic excitation activates the high-threshold Ca_L channels; the mean Ca^{2+} concentration inside the cell increases; this slowly activates the $K_{AHP}(Ca)$ conductance and decreases spike frequency (Fig. 3).

We have investigated the specific roles of different channels for spike frequency adaptation. The dependence of maximal (f_{max}) and steady state (f_∞) spike frequencies on input synaptic stimulation for neuron type I is shown in Fig. 4, *A–C*. Variations of maximal conductances of both $K_{AHP}(Ca)$ and Ca_L channels cause similar effects on spike frequency and adaptation. Figure 4, *A* and *B*, shows that an increase in either conductance does not influence f_{max} significantly but decreases f_∞ and increases the degree of adaptation. The increase in $\bar{g}_{AHP}$ causes a direct effect on the neuronal membrane behavior without changing $[Ca^{2+}]_{in}$, whereas the increase in $\bar{g}_{CaL}$ produces an increase in g_{AHP} due to the increase in $[Ca^{2+}]_{in}$.

Because the respiratory phases are relatively long (e.g., 500–2,000 ms) it is important that models of respiratory neurons with adapting patterns (e.g., early-I, post-I, and dec-E) adapt over considerable time. An analysis shows that in neuron type I the time constant of spike frequency adaptation depends strongly on the activation time constant of $K_{AHP}(Ca)$ conductance, τ_{mAHP}, and on the time constant of the calcium pump, τ_{pump}. The values of $\bar{g}_{AHP}$ and $\bar{g}_{CaL}$ also play an important role (Fig. 5) because an increase in their maximal conductances decreases the time constant of spike frequency adaptation but increases the degree of adaptation.

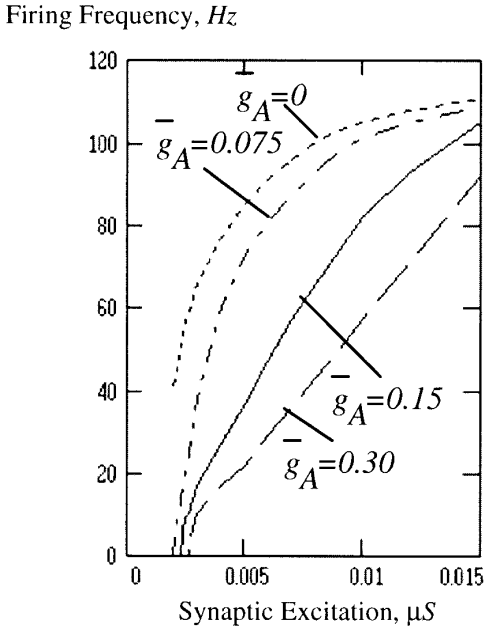

FIG. 2. Firing frequency characteristics of basic neuron model at different values of maximal conductance of K_A channels, $\bar{g}_A$ (μS).

TABLE 3. *Maximal conductances of ionic channels in the adapting (type I) and ramp firing (type II) respiratory neuron types*

	Maximal Conductance, $\bar{g}_i$, μS						
Type of Neuron	$\bar{g}_{Na}$	$\bar{g}_{DR}$	$\bar{g}_{A}$	$\bar{g}_{AHP}$	$\bar{g}_{CaL}$	$\bar{g}_{CaT}$	$\hat{g}_{L}$
Type I	3.0	0.9	0.15	0.15	0.0015	0	0.01
Type II	3.0	0.9	0.15	0.15	0	0.0025	0.01

This occurs because the lowered steady state firing frequency reduces the calcium influx per time unit, and hence the mean level of $[Ca^{2+}]_{in}$ impedes the efficacy of g_{AHP}. Unlike $\bar{g}_{AHP}$ and $\bar{g}_{CaL}$, an increase in $\bar{g}_{A}$ reduces the initial spike frequencies of the neuron (Fig. 4*C*).

It was assumed that $K_{AHP}(Ca)$ conductance regulates the adapting discharge patterns of respiratory neurons (specifically, early-I and post-I) (Champagnat and Richter 1994; Mifflin et al. 1985; Pierrefiche et al. 1995; Richter et al. 1986b, 1993). It is activated by free calcium ions, which accumulate intracellulary resulting from a Ca^{2+} influx via voltage-dependent calcium channels. Because this mechanism provides the adapting firing patterns in neuron type I, this neuron model has been used in our respiratory network models for simulating all adapting neurons (e.g., early-I, post-I, dec-E neurons).

A ramp firing neuron (type II): the role of Ca_T, $K_{AHP}(Ca)$, and K_A channels

Neuron type II was constructed by incorporating low-threshold Ca_T channels into the basic neuron model (Table 3). We have found that the low-threshold Ca_T channels together with $K_{AHP}(Ca)$ channels allow a *spike frequency augmenting (ramp firing) response* after release from hyperpolarization under conditions of constant synaptic excitatory drive. To be sure that this result is not specifically dependent on the particular formal description of the Ca_T conductance (see Table 1), we used other formal descriptions (e.g., taken from Schwaber et al. 1993) and obtained similar results. To optimize ramp firing behavior, the value of maximal conductance for Ca_T channels was set at $\bar{g}_{CaT} = 0.0025$ μS.

Neuron type II displays the following three types of ramp firing responses: *1*) immediate ramping (Fig. 6*A*), characterized by the ramp firing response immediately after the release from inhibition; *2*) rebound ramping (Fig. 6*B*), including an initial single rebound spike followed by a period of silence before the onset of ramp frequency firing; and *3*) delayed ramping (Fig. 6*C*), which differs from the rebound ramping by the lack of rebound excitation. These types of ramp firing patterns closely reflect firing patterns of ramp-I and E2 neurons recorded intracellulary in vivo (compare Fig. 6, *A–C*, with Fig. 1, *A–D*). The exact firing pattern is dependent on the amount of excitatory synaptic drive and the amplitude and duration of preceding synaptic inhibition. Thus it can be transformed from one type to the other by altering excitatory or inhibitory synaptic inputs.

The mechanism for ramp frequency firing is dependent on a preceding membrane hyperpolarization, which activates the low-threshold Ca_T (and K_A) channels. Subsequent release from the hyperpolarized state causes a rapid influx of calcium ions into the cell: this is sometimes sufficient to reach the activation voltage of sodium channels and produce rebound spiking (Fig. 6, *A* and *B*). The $[Ca^{2+}]_{in}$ increases (as a result of Ca_T current activation) and rapidly activates the $K_{AHP}(Ca)$ channels, which reduce cellular excitability (Fig. 6*A*) and delay the onset of discharge (Fig. 6, *B* and *C*). The activation of the $K_{AHP}(Ca)$ channels slowly decays, allowing an increase in spike frequency. We have found that the existence and duration of the delay before the onset of ramp firing pattern (Fig. 6, *B* and *C*) depends on the relationship between the amplitude of excitatory synaptic drive and the degree of activation of the $K_{AHP}(Ca)$ conductance, which is dependent on amount and duration of preceding inhibition.

The shaping of the ramp firing pattern, especially during a short period after the release from a hyperpolarized state, also was found to be dependent on K_A channels. Activation of K_A current either reduces or abolishes rebound spiking (Fig. 6*C*). If $\bar{g}_A$ is too small more than one rebound spike can be elicited in the rebound ramping pattern. In fact, the type of response pattern: rebound (as in Fig. 6*B*) or delayed (as in Fig. 6*C*) depends on the activation kinetics of Ca_T, or $K_{AHP}(Ca)$, or K_A conductances after release from inhibition. Because of this, the type of ramp firing pattern depends on the time constant with which the preceding synaptic inhibition is removed (τ_I^-).

We have investigated the dependence of the ramp firing pattern on the amount of synaptic excitation and inhibition, the maximal conductances of different channels, and the time constant of the release from inhibition (Fig. 7, *A–D*). The plots in the *middle* column of Fig. 7 are the same and correspond to data in Table 3 for neuron type II and $\tau_I^- = 15$ ms. Each row shows how the bifurcation borders between the regions for three different ramp firing patterns alter if one of the parameters changes. In general, a decrease in synaptic excitation and/or an increase in the preceding synaptic inhibition causes a transition from immediate ramping (A regions) to rebound ramping (B regions) and then to delayed ramping (C regions). The increase in maximal conductance of Ca_T, or $K_{AHP}(Ca)$, or K_A channels shifts the bifurcation border between the rebound ramping region (B) and the delayed ramping region (C) to stronger values of synaptic excitation and weaker values of preceding synaptic inhibition (Fig. 7, *A–C*).

The increase in the time constant of release from inhibition reduces the region of rebound ramping (Fig. 7*D*). A decrease of this time constant widens the region for rebound ramping and reduces the region for delayed ramping. Thus the kinetics of the release from inhibition play a significant role in determining the firing pattern.

Figure 8, *A–C*, shows the factors controlling the main parameters of the rebound ramping pattern: slope of firing frequency and delay between the rebound spike and the onset of ramp frequency discharge. An increase in excitatory input increases the initial slope of spike frequency and decreases the duration of the delay (Fig. 8, *A–C*). This is important for simulating inspiratory neuron activity because an increase in excitatory synaptic drive elicits an increase in the ramp of firing pattern of both inspiratory neurons and phrenic discharge (Botros and Bruce 1990; Feldman 1986; von Euler

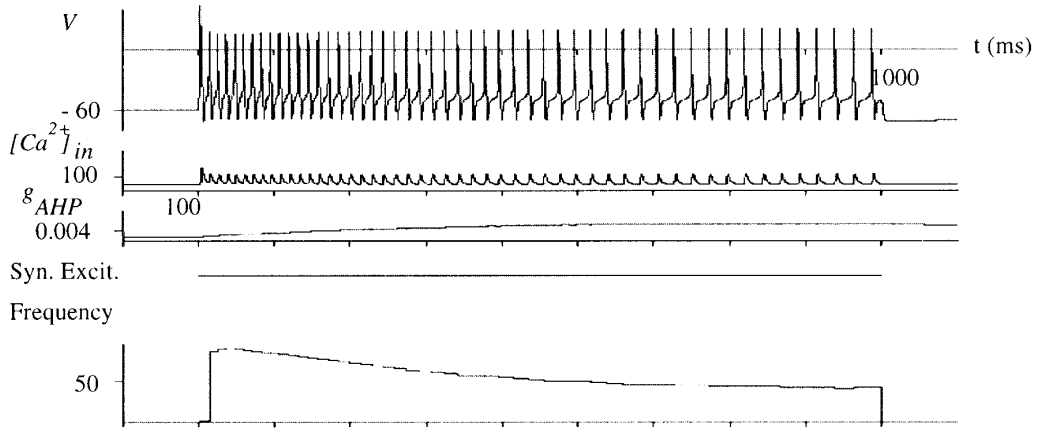

FIG. 3. Response of neuron type I to a stepwise excitatory synaptic input (In_E = 0.012 μS).

1986). An increase in the values of $\bar{g}_{CaT}$ or $\bar{g}_{AHP}$ increases the delay, whereas changing $\bar{g}_A$ is without effect (Fig. 8, *A–C, right*). Thus the delay in the model results from a combined influence of Ca_T and $K_{AHP}(Ca)$ channels. In contrast, the initial slope of firing frequency changes very little when $\bar{g}_{CaT}$ or $\bar{g}_{AHP}$ is varied, but decreases with an increase of $\bar{g}_A$ (Fig. 8, *A–C, left*). Thus activation of K_A channels allows a slower rate of rise of spike frequency.

The rebound membrane depolarization demonstrated by inspiratory and expiratory neurons after release from synaptic inhibition is reported to result from Ca_T channels (Richter et al. 1993) (Fig. 1, *B* and *C*). These channels slowly inactivate after release from hyperpolarization. The period of silence that characteristically follows the rebound spike (Fig. 1*A* for ramp-I, Fig. 1*B*) and delayed onset of discharge in ramp-I neurons can result from a shunting action by $K^+(Ca)$ current. This is the mechanism that operates in neuron type II. In addition, the same mechanism provides ramp firing patterns, because $K_{AHP}(Ca)$ conductance increases quickly with the increase of intracellular free Ca^{2+} concentration (caused by the Ca_T current) and then slowly decays. Consequently, neuron type II model has been used in our respiratory network models for simulating ramp-I and E2 neurons, which show similar ramp firing patterns during inspiration and stage II expiration, respectively.

DISCUSSION

We found that neuron models incorporating known membrane properties of neurons from respiratory related areas of brain stem and intrinsic dynamics of different calcium channels can produce the ramp firing and adapting patterns observed in respiratory neurons in vivo. Our finding that a ramp firing pattern can result from intrinsic membrane

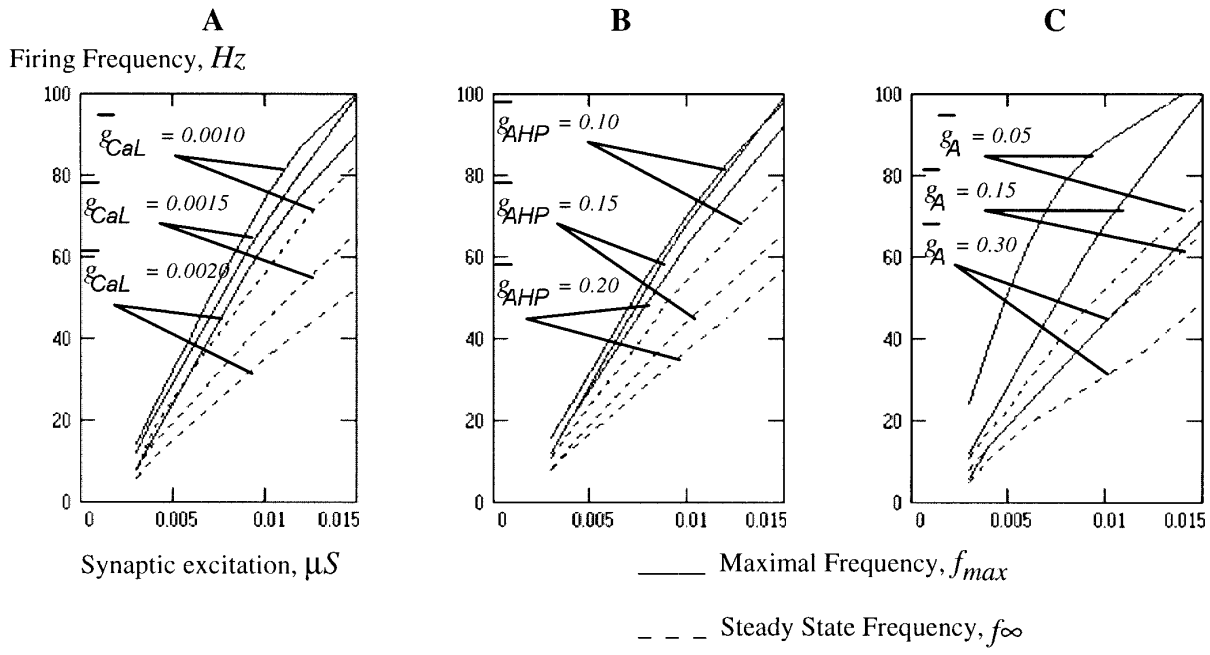

FIG. 4. Dependence of maximal (f_{max}) and steady state (f_∞) discharge frequencies on synaptic excitatory drive for neuron type I at different values of maximal conductances of Ca_L channels, g_{CaL}, (*A*); $K_{AHP}(Ca)$ channels, g_{AHP}, (*B*); and K_A channels, $\bar{g}_A$, (*C*).

properties, specifically from the combined influence of $K_{AHP}(Ca)$, Ca_T and K_A conductances, allows the hypothesis that the ramp firing patterns of inspiratory and expiratory neurons are based, in part, on the intrinsic membrane properties of these neurons.

We consider the explanation of ramp frequency discharges as a key point in understanding the neurogenesis of the respiratory pattern. As described in the INTRODUCTION the pattern in ramp-I neurons could result from collateral self-excitation or mutual synaptic excitation between the neurons of the same group (Botros and Bruce 1990; Feldman and Cowan 1975; Gottschalk et al. 1994; Ogilvie et al. 1992). However, in contrast to our hypothesis, this idea fails to explain *1*) the rebound ramping pattern (as in Fig. 1*A* for ramp-I or in Fig. 1*B*), because the rebound spikes would cause a self-excitation instead of the observed period of silence (see Fig. 1), and *2*) the observation that the ramp firing pattern in ramp-I neurons always follows release from a hyperpolarized state. In addition, positive feedback formed by self- or mutual-excitatory connections should reduce the operating range of the respiratory network and destabilize network behavior under some conditions. Thus our hypothesis gives a more plausible explanation for the ramp firing patterns of inspiratory neurons than the idea of self- or mutual excitation. We assume that the above intrinsic mechanism also can participate in shaping the ramp firing patterns of expiratory neurons.

Our simulation showed that the kinetics of release from inhibition play a significant role in determining the ramp firing pattern. This is a novel finding and has not been considered as a factor controlling neuronal firing behavior.

We showed that the adapting activity pattern of neuron type I, which is considered as a model of the adapting respiratory neurons (early-I, post-I, dec-E), is controlled by the interactions of $K_{AHP}(Ca)$ and Ca_L channels via the $[Ca^{2+}]_{in}$ dynamics. Alternatively, the ramp firing pattern of neuron type II, which is considered as a model of the ramp firing respiratory neurons (ramp-I and aug-E), originates from the combined influence of Ca_T, $K_{AHP}(Ca)$, and K_A channels and synaptic input providing the preceding inhibition. It was of interest that $K_{AHP}(Ca)$ channels in combination with Ca_L channels produced a spike frequency adaptation during synaptic excitation, but in combination with Ca_T channels, caused a ramp firing response following the release from inhibition. This prompts the hypothesis that the main difference between the respiratory neurons that adapt (e.g., early-I, post-I, and dec-E) and those that show ramp firing patterns (e.g., ramp-I and aug-E) reflects the ratio of two types of calcium channels: Ca_L channels predominate in adapting neurons, whereas Ca_T channels prevail in ramp firing neuron types.

Based on our hypothesis and modeling results we predict that selective blockade of the Ca_L current would decrease adaptation but should not influence the ramp firing patterns. In contrast, selective blockade of the Ca_T current may change the ramp firing patterns to high-frequency discharges but should not influence adaptation. Finally, blockade of either $K_{AHP}(Ca)$ channels or calcium accumulation inside the cell should reduce frequency changes in both discharge patterns resulting in a constant high-frequency response.

The transient potassium-A (K_A) channels also may play a role in shaping the specific patterns of respiratory neurons. One functional property of the potassium-A current is to permit a low firing frequency activity and a linear frequency-stimulus relationship (Connor and Stevens 1977). Another property of K_A channels is that their conductance inactivates slowly after depolarization from hyperpolarized levels and can delay firing depending on the amount and duration of the preceding inhibition (Dekin and Getting 1987; Haddad and Getting 1989). Because K_A and Ca_T channels have similar kinetic properties but differ in their influence on membrane behavior, there is a complex interaction between these channels just after release from hyperpolarization (Dekin and Getting 1987; McCormick and Huguenard 1992; Richter et al. 1985). However, most authors consider this feature of K_A channels unimportant for respiratory network performance because the neurons are not thought to be hyperpolarized strongly enough to activate this property (Champagnat et al. 1986b,c; Richter et al. 1986b). Our simulation showed that K_A channels can play a definite role in respiratory neuron

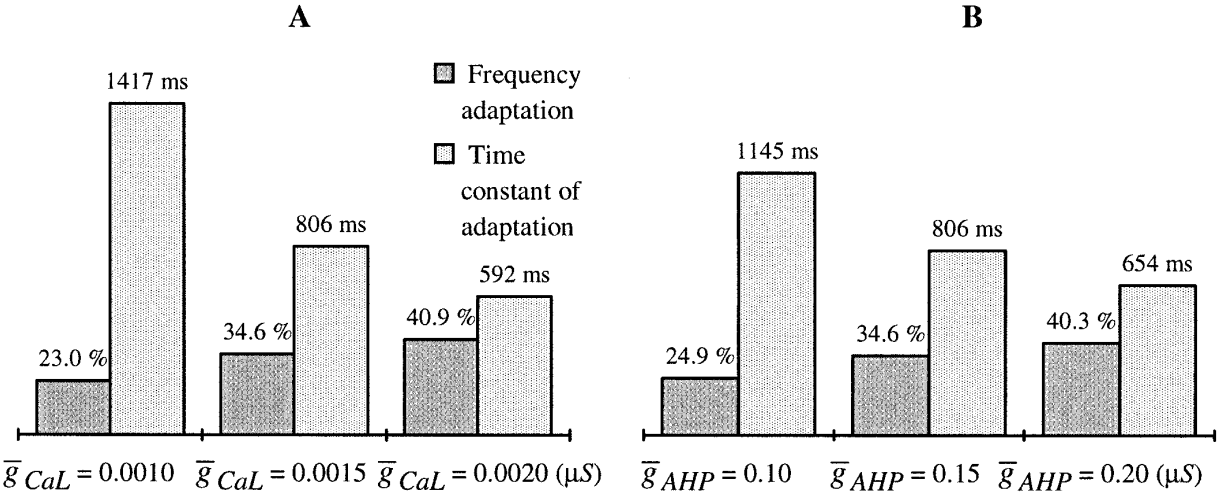

FIG. 5. Degree of frequency adaptation (calculated as $(1 - f_\infty/f_{max}) \cdot 100\%$) and adaptation time constant of neuron type I at different values of maximal conductances of Ca_L channels, g_{CaL}, (*A*), and $K_{AHP}(Ca)$ channels, g_{AHP}, (*B*); (In_E = 0.012 μS).

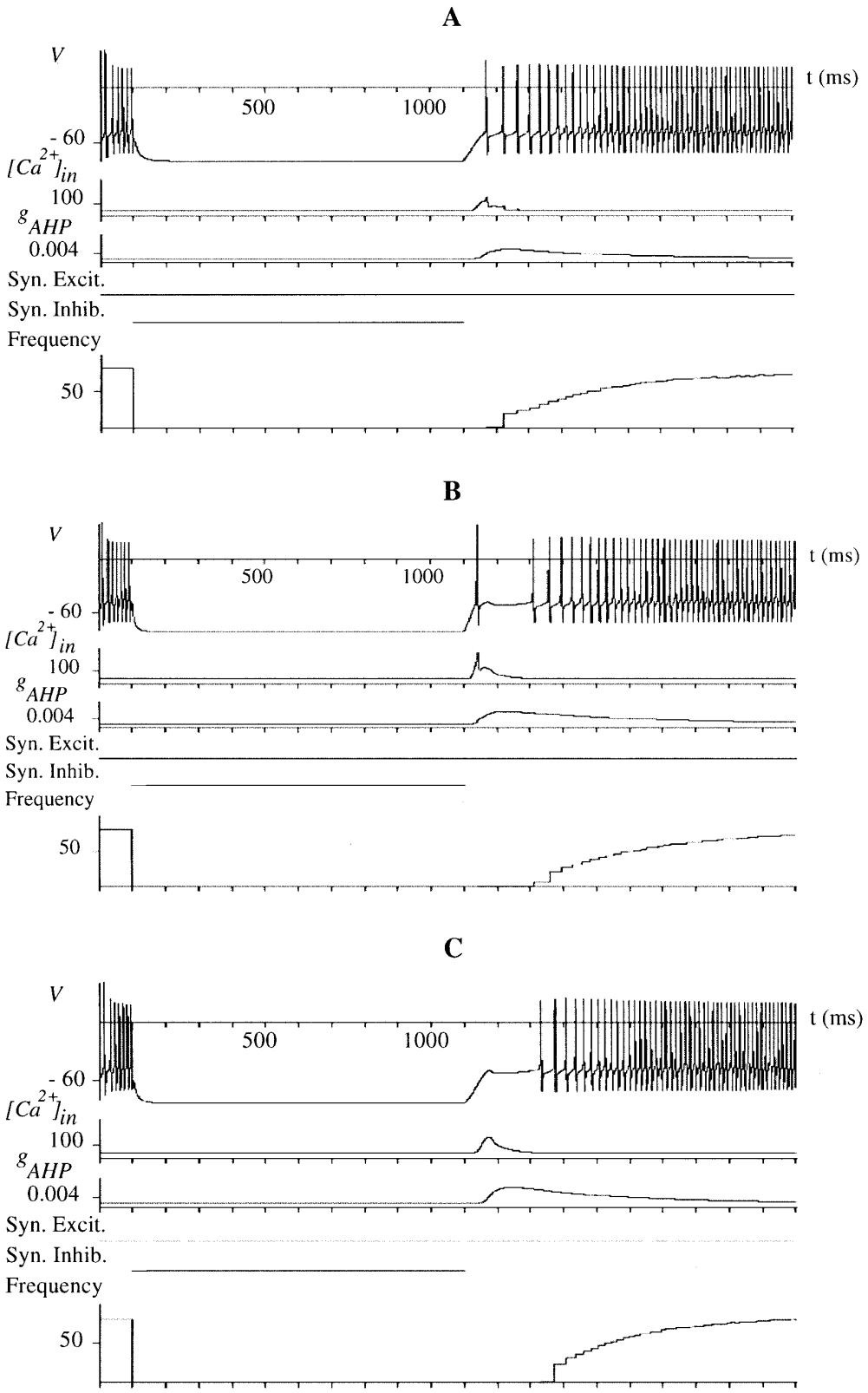

FIG. 6. Three types of ramp firing pattern of neuron type II after release from synaptic inhibition under conditions of constant synaptic excitatory drive. Three different ramp firing patterns were observed. *A*: immediate ramping (In_E = 0.009 μS; In_I = 0.06 μS; τ_I^- = 15 ms). *B*: rebound ramping (In_E = 0.009 μS; In_I = 0.08μS; τ_I^- = 15 ms). *C*: delayed ramping (In_E = 0.009 μS; IN_I = 0.13 μS; τ_I^- = 15 ms).

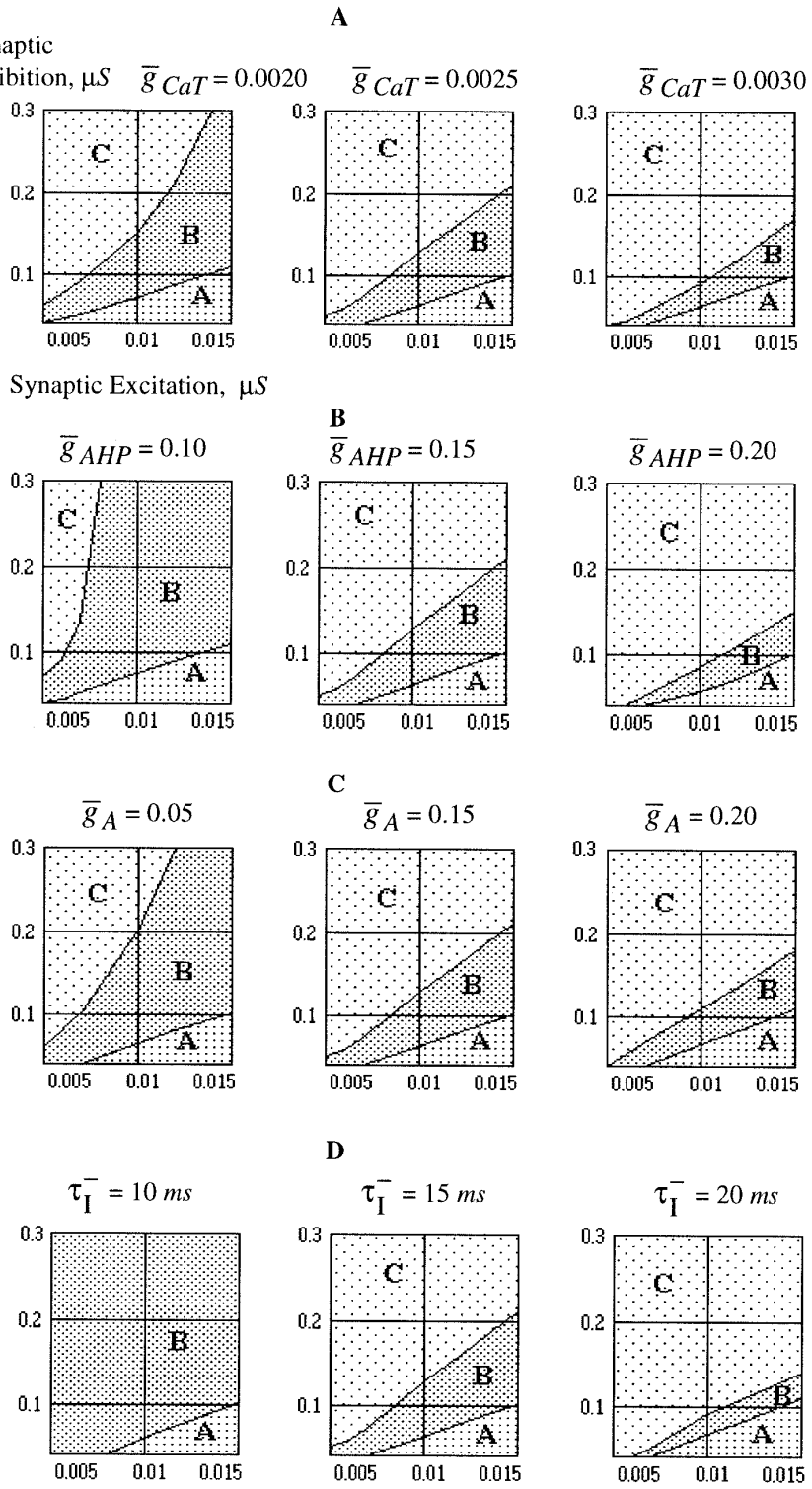

FIG. 7. Bifurcation borders between regions corresponding to 3 types of ramp firing pattern in neuron type II (see Fig. 6, *A–C*) in 2-dimensional space of synaptic excitation (abscissa) and inhibition (ordinate). All *middle* plots are the same and correspond to values of parameters in Table 3. In all plots, A, B, and C indicate regions that correspond to patterns in Fig. 6, *A*, *B*, and *C*, respectively. Borders alternate with variations of maximal conductances of Ca_T channels, $\bar{g}_{CaT}$, (*A*); K_{AHP}(Ca) channels, g_{AHP}, (*B*); K_A channels, g_A (*C*); and with changes of τ_I^- (*D*).

firing patterns by stabilizing and maintaining a low, steady state, firing frequency after adaptation and influencing the rebound excitation and initial firing frequency in the neurons with ramp firing patterns.

In the framework of a network paradigm, oscillations in the respiratory network occur because of sequential switching between different phases of activity. The timing of switches and durations of respiratory phases depend on both network properties (weights of synaptic interconnections) and intrinsic properties of respiratory neurons that control their adapting and ramp firing patterns. Because the dynamics of intracellular calcium and K_{AHP}(Ca) conductance are the main factors that define both slow adapting and slow augmenting patterns in different respiratory neurons, they are the key cellular factors that, together with network properties, control both the durations of respiratory phases and

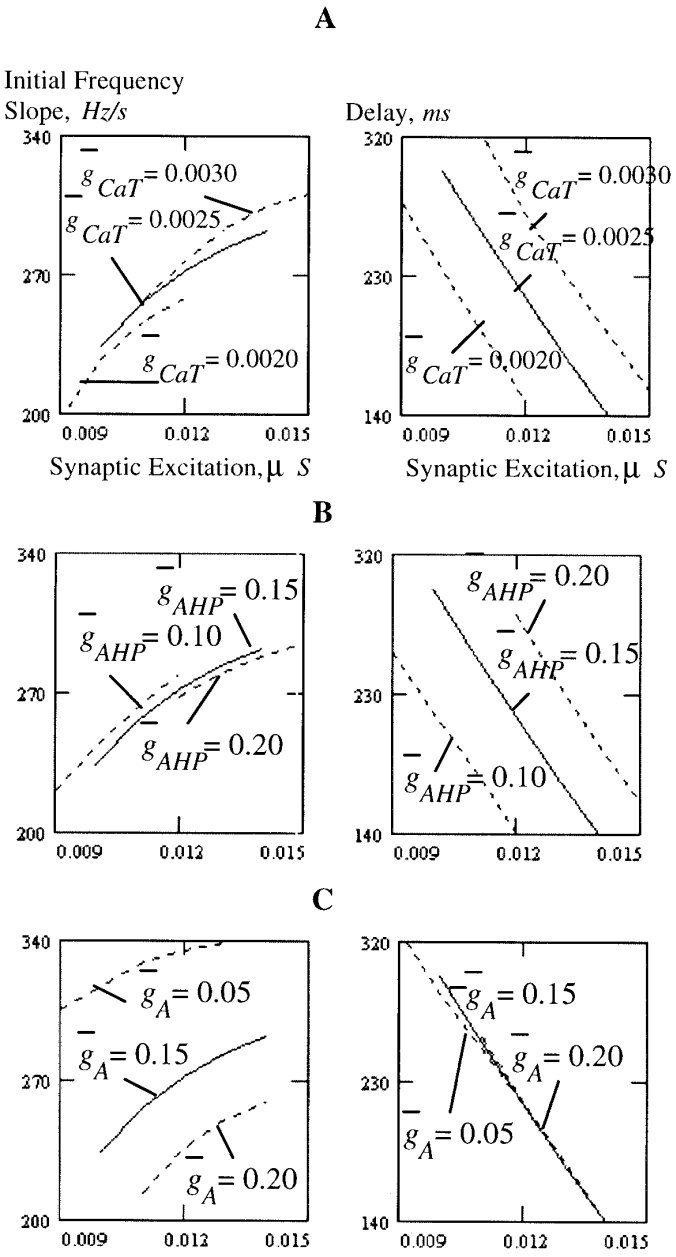

FIG. 8. Effect of altering excitatory synaptic drive on initial firing frequency slope (*left*) and delay before onset of firing (*right*) for rebound ramping pattern of neuron type II (Fig. 6*B*) at different values of maximal conductances of the Ca_T channels, $\bar{g}_{CaT}$, (*A*); K_{AHP}(Ca) channels, $\bar{g}_{AHP}$, (*B*); and K_A channels, $\bar{g}_A$, (*C*).

switching between them. This is consistent with the conclusion that the calcium-dependent potassium conductance controls respiratory phase durations by regulating the degree of adaptation of early-I and post-I neurons (Champagnat and Richter 1994; Champagnat et al. 1986b; Pierrefiche et al. 1995; Richter et al. 1985, 1986b, 1993).

In conclusion, our simulations have provided unique insights into the possible significance of intrinsic neuronal properties for neural mechanisms underlying respiratory network performance. The data presented here have prompted several hypotheses that await experimental investigation. The models of single respiratory neurons have been used in our respiratory network models, which are presented in the subsequent papers.

The authors are grateful to Dr. Jean Champagnat for comments and helpful discussion of the results in light of modern data on properties of respiratory neurons and to Drs. Y. Fuentes, B. A. Ogunnaike, K. F. Morris, and M. Pottmann for useful discussion of the models.

This research was supported by National Science Foundation Grant BIR93-153-03, Air Force Grant F49620-93-1-0285, and E. I. du Pont de Nemours. J. F. R. Paton holds a British Heart Foundation Lectureship.

Address reprint requests to I. A. Rybak.

Received 8 April 1996; accepted in final form 12 December 1996.

REFERENCES

BALIS, U. J., MORRIS, K. F., KOLESKI, J., AND LINDSEY, B. G. Simulations of a ventrolateral medullary neural network for respiratory rhythmogenesis inferred spike train cross-correlation. *Biol. Cybern.* 70: 311–327, 1994.

BOTROS, S. M. AND BRUCE, E. N. Neural network implementation of the three-phase model of respiratory rhythm generation. *Biol. Cybern.* 63: 143–153, 1990.

BRYANT, T. H., YOSHIDA, S., DE CASTRO, D., AND LIPSKI, J. Expiratory neurons of the Bötzinger complex in the rat: a morphological study following intracellular labeling with biocytin. *J. Comp. Neurol*. 335: 267–282, 1993.

CHAMPAGNAT, J., DENAVIT-SAUBIE, M., GRANT, K., AND SHEN, K. F. Organization of synaptic transmission in the mammalian solitary complex, studied in vivo. *J. Physiol. Lond.* 381: 551–573, 1986a.

CHAMPAGNAT, J., JACQUIN, T., AND RICHTER, D. W. Voltage-dependent currents in neurons of the nuclei of the solitary tract of rat brain stem slices. *Pfluegers Arch.* 406: 372–379, 1986b.

CHAMPAGNAT, J. AND RICHTER, D. W.The roles of K conductance in expiratory pattern generation in anaesthetized cats. *J. Physiol. Lond.* 479: 127–138, 1994.

CHAMPAGNAT, J., RICHTER, D. W., JACQUIN, T., AND DENAVIT-SAUBIE, M. Voltage-dependent conductances in neurons of the ventrolateral NTS in rat brain stem slices. In: *Neurobiology of the Control of Breathing*, edited by C. von Euler and H. Langercrantz. New York: Raven, 1986c, p. 217–221.

CONNOR, J. A. AND STEVENS, C. F. Predictions of repetitive firing behavior from voltage-clamp data on an isolated neurone soma. *J. Physiol. Lond.* 213: 31–53, 1977.

DEKIN, M. S. AND GETTING, P. A. In vitro characterization of neurons in the ventral part of the nucleus tractus solitarius. II. Ionic basis for repetitive firing patterns. *J. Neurophysiol*. 58: 215–229, 1987.

DUFFIN, J. A model of respiratory rhythm generation. *Neuroreport* 2: 623–626, 1991.

DUFFIN, J. A., EZURE, K., AND LIPSKI, J. Breathing rhythm generation: focus on the rostral ventrolateral medulla. *News Physiol. Sci*. 10: 133–140, 1995.

ECKERT, R. AND CHAD, J. E. Inactivation of Ca channels. *Prog. Biophys. Mol. Biol.* 44: 215–267, 1984.

EZURE, K. Synaptic connections between medullary respiratory neurons and consideration on the genesis of respiratory rhythm. *Prog. Neurobiol.* 35: 429–450, 1990.

FELDMAN, J. L. Neurophysiology of breathing in mammals. In: *Handbook of Physiology. The Nervous System. Intrinsic Regulatory Systems of the Brain.* Bethesda, MD: Am. Physiol. Soc., 1986, sect. I, vol. IV, p. 463–524.

FELDMAN, J. L. AND CLELAND, C. L. Possible roles of pacemaker neurons in mammalian respiratory rhythmogenesis. In: *Cellular Pacemakers*, edited by D. O. Carpenter. New York: Wiley, 1982, vol. 2, p. 101–119.

FELDMAN, J. L. AND COWAN, J. D. Large scale activity in neural net. II. A model for the brain stem respiratory oscillator. *Biol. Cybern.* 17: 39–51, 1975.

GEMAN, S. AND MILLER, M. Computer simulation of brain stem respiratory activity. *J. Appl. Physiol.* 41: 931–938, 1976.

GOTTSCHALK, A., OGILVIE, M. D., RICHTER, D. W., AND PACK, A. I. Computational aspects of the respiratory pattern generator. *Neural Comput.* 6: 56–68, 1994.

HADDAD, G. G. AND GETTING, P. A. Repetitive firing properties of neurons in the ventral region of nucleus tractus solitarius. In vitro studies in adult and neonatal rat. *J. Neurophysiol.* 66: 1213–1223, 1989.

HILLE, B. *Ionic Channels of Excitable Membranes*. Sunderland, MA: Sinauer, 1984.

HODGKIN, A. L. AND HUXLEY, A. F. A quantitative description of membrane current and its application to conduction and excitation in nerve. *J. Physiol. Lond*. 117: 500–544, 1952.

HUGUENARD, J. R. AND MCCORMICK, D. A. *Vclamp and Cclamp. A Computational Simulation of Single Thalamic Relay and Cortical Pyramidal Neurons. Neural Simulation Instruction Manual*. Stanford, CA: Stanford Univ., 1991.

HUGUENDARD, J. R. AND MCCORMICK, D. A. Simulation of the currents involved in rhythm oscillations in thalamic relay neurons. *J. Neurophysiol.* 68: 1373–1383, 1992.

KLAGES, S., BELLINGHAM, M. C., AND RICHTER, D. W. Late expiratory inhibition of stage 2 expiratory neurons in the cat—a correlate of expiratory termination. *J. Physiol. Lond.* 70: 1307–1315, 1993.

KREUTER, F., RICHTER, D. W., CAMERER, H., AND SENEKOWITSCH, R. Morphological and electrical description of medullary respiratory neurons of the cat. *Pfluegers Arch.* 372: 7–16, 1977.

LUMSDEN, T. Observations on the respiratory centers in the cat. *J. Physiol. Lond.* 57: 153–160, 1923.

MACGREGOR, R. I. *Neural and Brain Modeling*. New York: Academic, 1987.

MCCORMICK, D. A. AND HUGUENARD, J. R. A model of the electrophysiological properties of thalamocortical relay neurons. *J. Neurophysiol.* 68: 1384–1400, 1992.

MIFFLIN, S., BALLANTYNE, D., BACKMAN, S., AND RICHTER, D. W. Evidence for a calcium-activated potassium conductance in medullary respiratory neurons. In: *Nerogenesis of Central Respiratory Rhythm*, edited by A. M. Bianchi and M. Denvait-Saubie. Lancaster, UK: MTP, 1985, p. 179–182.

OGILVIE, M. D., GOTTSCHALK, A., ANDERS, K., RICHTER, D. W., AND PACK, A. I. A network model of respiratory rhythmogenesis. *Am. J. Physiol.* 263 (*Regulatory Integrative Comp. Physiol.* 31): R962–R975, 1992.

PATON, J.F.R. The ventral medullary respiratory network of the mature mouse studied in a working heart-brain stem preparation. *J. Physiol. Lond.* 493: 819–831, 1996.

PIERREFICHE, O., CHAMPAGNAT, J., AND RICHTER, D. W. Calcium-dependent conductances control neurones involved in termination of inspiration in cats. *Neurosci. Lett*. 184: 101–104, 1995.

PIERREFICHE, O., FOUTZ, A. S., AND DENAVAIT-SAUBIE, M. Effects of receptor agonists and antagonists on the bulbar respiratory network in cat. *Brain Res.* 605: 77–84, 1993.

RICHTER, D. W. AND BALLANTYNE, D. A three phase theory about the basic respiratory pattern generator. In: *Central Neurone Environment*, edited by M. Schlafke, H. Koepchen, and W. See. Berlin: Springer, 1983, p. 164–174.

RICHTER, D. W., BALLANTYNE, D., AND MIFFLIN, S. Interaction between postsynaptic activities and membrane properties in medullary respiratory neurons. In: *Nerogenesis of Central Respiratory Rhythm*, edited by A. M. Bianchi and M. Denvait-Saubie. Lancaster, UK: MTP, 1985, p. 172–178.

RICHTER, D., BALLANTYNE, D., AND REMMERS, J. E. How is the respiratory rhythm generated? A model. *News Physiol. Sci*. 1: 109–112, 1986a.

RICHTER, D. W., CHAMPAGNAT, J., JACQUIN, T., AND BENACKA, R. Calcium currents and calcium-dependent potassium currents in mammalian medullary respiratory neurons. *J. Physiol. Lond.* 470: 23–33, 1993.

RICHTER, D. W., CHAMPAGNAT, J. S., AND MIFFLIN, S. W. Membrane properties involved in respiratory rhythm generation. In: *Neurobiology of the Control of Breathing*, edited by C. von Euler and H. Langercrantz. New York: Raven, 1986b, p. 141–147.

RICHTER, D. W. Neural regulation of respiration: rhythmogenesis and afferent control. In: *Comprehensive Human Physiology*, edited by R. Greger and U. Windhorst. Berlin: Springer-Verlag, 1996, vol. II, p. 2079–2095.

RUBIO, J. E. A new mathematical model of the respiratory center. *Bull. Math. Biophys.* 34: 467–481, 1972.

SCHWABER, J. S., GRAVES, E. B., AND PATON, J.F.R. Computational modeling of neuronal dynamics for systems analysis: application to cardiovascular NTS neurons in the rat. *Brain Res*. 604: 126–141, 1993.

SCHWARZACHER, S. W., WILHEM, Z., ANDERS, K., AND RICHTER, D. W. The medullary respiratory network in the rat. *J. Physiol. Lond.* 435: 631–644, 1991.

SMITH, J. C., ELLENBERGER, H., BALLANYI, K., RICHTER, D. W., AND FELDMAN, J. L. Pre-Bötzinger complex: a brain stem region that may generate respiratory rhythm in mammals. *Science Wash. DC* 254: 726–729, 1991.

VON EULER, C. Brain stem mechanism for generation and control of breathing pattern. In: *Handbook of Physiology. The Respiratory System. Control of Breathing.* Washington, DC: Am. Physiol. Soc., 1986, sect. III, vol. II, p. 1–67.

YAMADA, W. M., KOCH, C., AND ADAMS, P. B. Multiple channel and calcium dynamics In: *Methods in Neuronal Modeling.* Cambridge: MIT, 1989, p. 97–133.